RANDOM-MODULATION DIFFERENTIAL ABSORPTION LIDAR BASED ON SEMICONDUCTOR LASERS AND SINGLE PHOTON COUNTING FOR ATMOSPHERIC CO_2 SENSING

M. Quatrevalet[1], X. Ai[2], A. Pérez-Serrano[3], P. Adamiec[4], J. Barbero[4], A. Fix[1], J. G. Rarity[2], G. Ehret[1] and I. Esquivias[3]
[1]Institut für Physik der Atmosphäre, DLR, Germany. [2]Dept.of Electrical and Electronic Engineering, University of Bristol, United Kingdom. [3]CEMDATIC-ETSI Telecomunicación, Universidad Politécnica de Madrid, Spain. [4]Alter Technology TÜV Nord S.A.U., Spain.

I. INTRODUCTION

Carbon dioxide (CO_2) is the major anthropogenic greenhouse gas contributing to global warming and climate change. Its concentration has recently reached the 400-ppm mark, representing a more than 40 % increase with respect to its level prior to the industrial revolution. However, the exchanges of CO_2 between the atmosphere and the natural or anthropogenic sources/sinks at the Earth's surface are still poorly quantified. A better understanding of these surface fluxes is required for appropriate policy making. At present, the concentrations of CO_2 are mainly measured in-situ at a number of surface stations that are unevenly distributed over the planet. Air-borne and space-borne missions have the potential to provide a denser and better distributed set of observations to complement this network. In addition to passive measurement techniques, the integrated path differential absorption (IPDA) lidar technique [1] has been found to be potentially suited for fulfilling the stringent observational requirements. It uses strong CO_2 absorption lines in the 1.57 or in the 2 μm region and the backscatter from the ground or a cloud top to measure the column averaged CO_2 mixing ratio (XCO_2) with high precision and accuracy. The European Space Agency (ESA), has studied this concept in the frame of the Advanced Space Carbon and Climate Observation of Planet Earth (A-SCOPE) mission in 2006. Although a lack of technological readiness prevented its selection for implementation, recommendations have been formulated to mature the instrument concept by pursuing technological efforts [2]. During the last years, a tremendous effort in the assessment of the optimal CO_2 active sensing methodology is being performed in the context of NASA mission Active Sensing of CO_2 Emissions over Nights, Days, and Season (ASCENDS) [3].

Space-borne lidar systems require laser transmitters with very good performance in terms of output power, beam quality, conversion efficiency, long term reliability and environmental compatibility. Additionally, spectral purity and stability are required for gas sensing. The availability of suitable laser sources is one of the main challenges in future space missions for accurate measurement of atmospheric CO_2. Typical laser sources currently used in lidar systems are solid state lasers working in pulsed regime [4]. Although these laser systems have demonstrated the high average power, high laser beam quality and frequency stability required by the application, it is at the expense of a bulky system with low wall plug efficiency, which is a main concern for space-borne applications. Recently, a new generation of high brightness semiconductor lasers based on tapered geometry has demonstrated relatively high average power levels together with a good beam quality [5]. These devices are emerging candidates for its direct use in space lidar systems because they have clear advantages over other laser types in terms of compactness and conversion efficiency. In addition, they present high reliability and good radiation hardness for most space applications. However, they cannot produce the high energy pulses needed in a standard pulsed IPDA lidar. Instead they are very well suited to intensity modulated continuous wave (IM-CW) techniques [6]. Among the different IM-CW techniques, in this work we pay attention on the Random Modulated Continuous Wave (RM-CW) approach [7], also called Pseudo-Random Noise (PRN) modulation. All IPDA techniques, both pulsed and IM-CW, can benefit by using Single Photon Counting (SPC) techniques in the receiver [8]. In fact, photomultiplier detectors have been used in pulsed systems [3] and HgCdTe Avalanche Photodiodes (APD) have been proposed for the application [9] due to their high sensitivity and low noise.

In this contribution we propose an IPDA lidar system based on semiconductor lasers and single photon counting detection for space-borne column-averaged measurements of atmospheric CO_2 in the context of European project BRITESPACE [10]. The design of the different elements of the fabricated prototype is discussed. Although it was initially planned to use two semiconductor lasers like the one shown in [5], due to technical problems the lidar system was completed with commercial DFB lasers and an EDFA. Co-located 2 km path-trial experiments with a pulsed system and in-situ measurements were performed for comparison. Our results show that this approach is a promising candidate to be used in space-borne lidar systems.

The paper is organized as follows. In Section II, the theoretical model of the RM-CW IPDA SPC lidar system is summarized and its space-borne implementation is briefly discussed. In Section III, the compact fabricated lidar instrument design is detailed. In Section IV, the experimental setup involving the CHARM-F pulsed system [11] and in-situ measurements is described. The obtained results are shown in Section V. Finally, the conclusions are drawn in Section VI.

II. THEORETICAL MODEL

An IPDA lidar can provide column-averaged CO_2 measurement by sounding the atmosphere at two wavelengths which are relevant for the gas under study: one wavelength is set near the center of a CO_2 absorption line (on-line channel, λ_{on}) and the other is set close to but off the same line (off-line channel, λ_{off}). Both wavelengths are close enough to exhibit almost identical aerosol attenuations, but will exhibit different CO_2 absorptions. The attenuation from CO_2 molecules can be calculated by the power ratio of the back-scattered signals at the end of the optical path and can be converted into a column-averaged mixing ratio thanks to the knowledge of the path length from the round-trip time delay. The Differential Absorption Optical Depth (*DAOD*) quantifies the molecular absorption by the CO_2 along the path between the scattering surface and the instrument. It can be written as

$$DAOD = \frac{1}{2}\ln\left(\frac{E_{on}\,R_{off}}{E_{off}\,R_{on}}\right) = \int_0^Z \left(\sigma_{on}(z) - \sigma_{off}(z)\right) n_{CO2}(z)dz\,, \tag{1}$$

where $E_{on,off}$ are the emitted on- and off-line energies, $R_{on,off}$ are the received on- and off-line echoes, n_{CO2} is the CO_2 density and $\sigma_{on,off}$ denotes the altitude dependent effective cross-section. In the particular case of using RM-CW, the transmitted signal is a Pseudo Random Bit Sequence (PRBS) as shown in Fig. 1 (a) composed by a Maximum Length Sequence (MLS). The off-line signal is delayed respect to the on-line signal in order to avoid cross-talk [12]. The *N*-bit PRBS can be represented as a $a[i] \in \{0,1\}$. Assuming single photon detection, the measurement of the cross-correlation $C[i]$ between the PRBS (the optical detected signal) with its bipolar sequence described by $a'[i] = 2a[i] - 1 \in \{-1,1\}$ (the electrical reference signal) for both on-line and off-line wavelengths provides the *DAOD*. When a PRBS $a[i]$ of the length $N = 2i_m$ is used for the on-line signal $a_{on} = a[i]$, the off-line code can be obtained by cyclically shifting the PRBS as $a_{off} = a[i - i_m]$. This approach allows the returns of both wavelengths to be separated and distinguishable in the cross-correlation result as shown in Fig. 1 (b). At the detector, apart from the signal counts, ambient light and detector dark counts are also collected. The combined cross-correlation result can be written as

$$C[i] = \left(n_{on}[i] + n_{off}[i] + n_{amb}[i] + n_{\det}[i]\right) \otimes a'[i]\,, \tag{2}$$

where

$$n_{on,off}[i] = 2\,P_{on,off}\,G_{on,off}\,T_c\,\eta_e\,a_{on,off}[i - \tau / T_c] \tag{3}$$

are the photo-electrons detected corresponding to the backscattered on- and off-line signals, $P_{on,off}$ is the initial average power of the on- and off-line transmitted signals, T_c is the bit time or chip-time, η_e denotes the conversion coefficient from incident photon numbers to detections of photo-electrons (including the optical and detector efficiencies) and

$$G_{on,off} = \alpha \frac{A_r}{Z^2} \mathrm{e}^{-2OD_{on,off}}\,, \tag{4}$$

with the total column optical path written as

$$OD_{on,off} = OD_0 + \int_0^Z \sigma_{on,off}(z)\, n_{co2}(z)dz\,, \tag{5}$$

where α is the albedo for the ground (approximated by a Lambertian surface), A_r is the receiving telescope area, Z is the target distance $Z = c\,\tau/2$, being τ the flight time, $OD_{on,off}$ denote the total column optical depth, including a losses wavelength-independent term OD_0. The total and differential absorptions are related through $DAOD = OD_{on} - OD_{off}$. The photo-electrons detected due to the ambient light read as

$$n_{amb} = \eta_e\,T_c\,L_s\,\Delta_\lambda\,A_s\,\frac{A_r}{Z^2}\mathrm{e}^{-OD_0}\,, \tag{6}$$

where L_s denotes the Nadir solar spectral radiance, Δ_λ represents the bandwidth of the optical filter at the detector; A_s is the ground surface area covered by the detector field-of-view, that relates to the receiver field-of-view θ_{fov} of the receiver by $A_s = 1/4\pi\theta_{fov}^2 Z^2$; A_r / Z^2 denotes the solid angle of the receiver telescope. The photo-electrons generated due to the detector's dark current read as

$$n_{\det} = k_{dc}\,T_c\,, \tag{7}$$

where k_{dc} is the detector dark count rate.

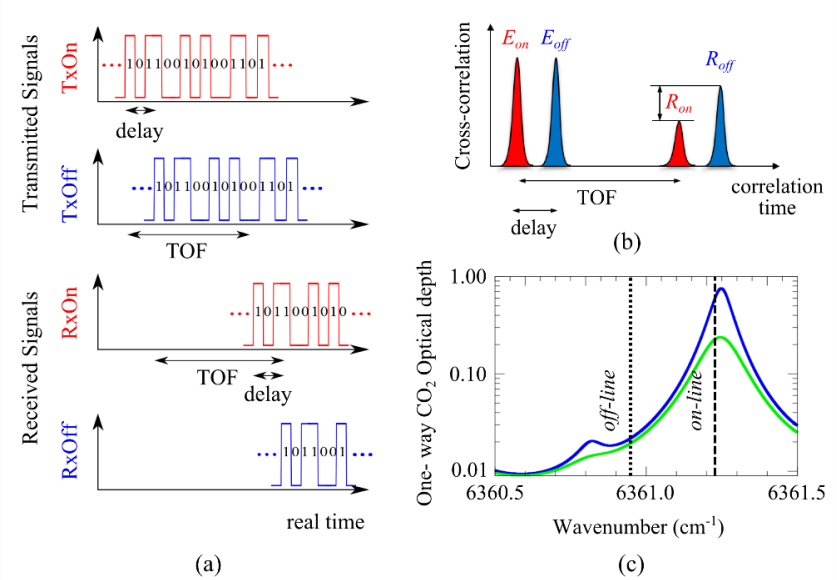

Fig. 1..(a) Pseudo-random bit sequences (PRBS) used in the random modulated continuous wave (RM-CW) lidar approach. TOF: Time of flight. (b) Differential absorption optical depth (DAOD) measurement from the RM-CW IPDA lidar systems. (c) CO_2 one-way optical depth seen from a space-borne instrument (blue) for a US standard atmosphere and on a 3 km horizontal path at ground level (green) for a pressure of 1013.15 hPa and a temperature of 273.13 K. The chosen CO_2 absorption line is at 6361.2506061 cm^{-1} (1572.01792843 nm) [13]. The on-line and off-line wavelengths are indicated with black dashed and dotted lines, respectively.

As shown in Fig. 1 (b), due to the correlation properties of the PRBS ($a[i] \otimes a'[i] \sim N/2\,\delta[i]$), the sample of the emitted energies are recoded at the initial bins as the photon numbers $E_{on,off}$, while the last returned bins record the total received photon number for the on and off-line wavelengths $R_{on,off}$. The latter can be written as

$$R_{on,off} = C_{on,off}[\tau/T_c] = N\,P_{on,off}\,G_{on,off}\,T_c\,\eta_e\,. \tag{8}$$

On the other hand, the total dark counts and ambient counts integrated in a cross-correlation bin can be further denoted as $R_{amb} = N\,n_{amb}$ and $R_{\det} = N\,n_{\det}$ respectively. The quantity of scientific interest, the dry-air volume mixing ratio of CO_2, vmr_{CO2}, is related to n_{CO2} and the density of dry air n_{air} via $vmr_{CO2}(z) = n_{CO2}(z)/n_{air}(z)$. In fact the obtained DAOD is proportional to a weighted average of vmr_{CO2} over the whole column which is referred as XCO_2,

$$XCO_2 = \int_0^Z vmr_{CO_2}(z)\frac{WF(z)}{\int_0^Z WF(z)dz}dz = \frac{DAOD}{IWF}, \tag{9}$$

where the weighting function WF is described by

$$WF(z) = n_{air}(z)\left(\sigma_{on}(z) - \sigma_{off}(z)\right), \tag{10}$$

where the density of air n_{air} can be obtained from the ideal gas law, and the altitude dependent cross-section $\sigma_{on,off}$ can be calculated from data obtained from the HITRAN database [14]. The details on the model developed based in a full-waveform simulation, where effects such as linewidth broadening, Doppler shift and topographic variations are included, can be found in [15]. To summarize, XCO_2 can be calculated from the following information: (a) the instrument measurement by the energy ratio of the received on- and off-line wavelengths; (b) the orbit altitude to the target distance Z, also derived from the lidar returns themselves; and (c) Numerical weather prediction and spectroscopic auxiliary data. By proper selection of the sounding on and off-line wavelengths possible measurement biases due to atmospheric water vapor can be significantly reduced [13].

The variance of the on-line at the peak of cross-correlation V_{on} and so forth for the off-line variance V_{off} is obtained as

$$V_{on,off} = R_{on,off} + R_{off,on} + R_{amb} + R_{det}\,. \tag{11}$$

Consequently on- and off-line SNRs can be estimated,

$$SNR_{on,off} = \frac{R_{on,off}}{\sqrt{R_{on,off} + R_{off,on} + R_{amb} + R_{\det}}}\,. \tag{12}$$

With the SNRs formulated, assuming Gaussian approximation to Poisson noise, the CO_2 retrieval precision can be estimated by Gaussian error propagation. The CO_2 detection precision can be simplified to

$$\Delta xco_2 = \sqrt{\left(\frac{\delta xco_2}{\delta R_{on}}\right)^2 V_{on} + \left(\frac{\delta xco_2}{\delta R_{off}}\right)^2 V_{off}} = \frac{\sqrt{SNR_{on}^{-2} + SNR_{off}^{-2}}}{2\,IWF}. \quad (13)$$

The theoretical model defines the CO_2 retrieval precision (random error) in relation to varying system parameters. An extensive study of the model led to a good understanding of the underlying principles, yielding to a baseline system configuration. To optimize a large set of related parameters, an initial condition was defined. This is set according to the intuitive understanding of the IPDA lidar approach with reference to pulsed systems from [1].

In summary, although the proposed scheme may be more susceptible to ambient and detector noise, for a low reflectivity case as given by the ocean surface, our calculations show a retrieval precision of 1.5 ppm over 50 km path integration can be achieved assuming existing technological readiness in a space-borne scenario. Advanced filtering technologies can be used to mitigate the ambient light problem allowing the retrieval precision to be improved to 0.5 ppm level. For more details we refer the reader to [15].

In the following, the design and on ground performance of a RM-CW SPC lidar system prototype is shown and discussed. One should notice that a 2 km on ground trial path presents differences with respect to a space-borne scenario. Fig. 1 (c) shows the difference between the one-way CO_2 optical depth in both scenarios and the chosen wavelengths for the on- and off-line signals. Moreover, speckle effects will be more important in the on ground scenario due to using a fixed target than in a space-borne scenario, where the satellite is moving and the target is continuously changing.

III. RM-CW SPC IPDA LIDAR SYSTEM

The design of the complete IPDA lidar system prototype is shown in Fig. 2 (a). It consists of the laser transmitter, the optics for beam transmission and reception, and the control electronics. The pan-tilt mounting allowed to vibrate the instrument, in order to slightly but continuously change the line-of-sight of the whole instrument, thereby changing the speckle pattern at the target.

A. Transmitter

The laser transmitter architecture is shown in the upper part of Fig. 2 (a). It provides two output beams: one is sent to the target and the other is used as reference and mixed with the received signal, for the calculation of the *DAOD*. It consists of two DFB lasers (one for each sounding frequency λ_{on}, λ_{off}), two acousto-optic modulators (AOMs), an EDFA, the control electronics and the frequency stabilization unit (FSU). A fraction of the output power of the two laser chips is sent to the FSU in order to stabilize the emission frequency. The other fraction is sent to an AOM where is non-return-to-zero (NRZ) modulated with the PRBS. We have used a chip time T_c = 40 ns corresponding to a bit rate of 25 Mb/s, providing us with a range resolution of 6 m. The length of the PRBS is $N = 2^{14} - 1 = 16383$, therefore the unambiguous range is 98.3 km. After the AOM, the two signals are combined and sent to a polarization scrambler (PS) avoiding the polarization dependent beam splitting to the reference path before being amplified by the EDFA (Keopsys KPS-STD-BT-L-30-PB-101-FA-FA). The average output power for each sounding frequency after the amplification stage is around 0.3 W. After being amplified a small fraction of the signal is sent to the integrated sphere to be used as reference by the receiver. The integrating sphere is used for beam homogenization and the rotational diffuser reduces the speckle noise in the references.

For accurate estimation of the gas molecule concentration, IPDA lidar systems require high frequency stabilization [1]. In this regard, the most critical frequency is the on-line, due to the slope in the wing of the line. The emission linewidth and the linewidth knowledge accuracy are expected to be uncritical for the proposed transmitter, because pseudo-random modulation dominates the linewidth which is therefore known, hence this broadening effect can be mitigated during data processing. In order to achieve the frequency stability requirements, we use two opto-electrical feedback loops, based on phase locking loops (PLLs) (LaseLock 4 Channel), for the stabilization of the on- and off-channels coupled to the output of a third opto-electrical feedback loop for CO_2 locking. The scheme of the FSU is shown in Fig. 2 (b). Light emitted from the on-line DFB laser is sent to the on-line locking feedback loop. In the same way, the light emitted from the off-line DFB laser is sent to the off-line locking feedback loop. We use a master DFB laser that is locked to the selected CO_2 absorption line using a single pass CO_2 reference cell and a custom feedback loop based on a commercially available laser frequency locking equipment. The measured master DFB stabilization range is around 18 kHz at the interval of 23 s, thus marking a limit on the on- and off-line wavelengths. The light emitted from the master laser is injected into the on- and off-line frequency locking loops and it is used to stabilize the beat note of the on-line and off-line signals with respect to the master laser frequency, with a tunable 350 MHz and with a fixed 10 GHz offsets, respectively.

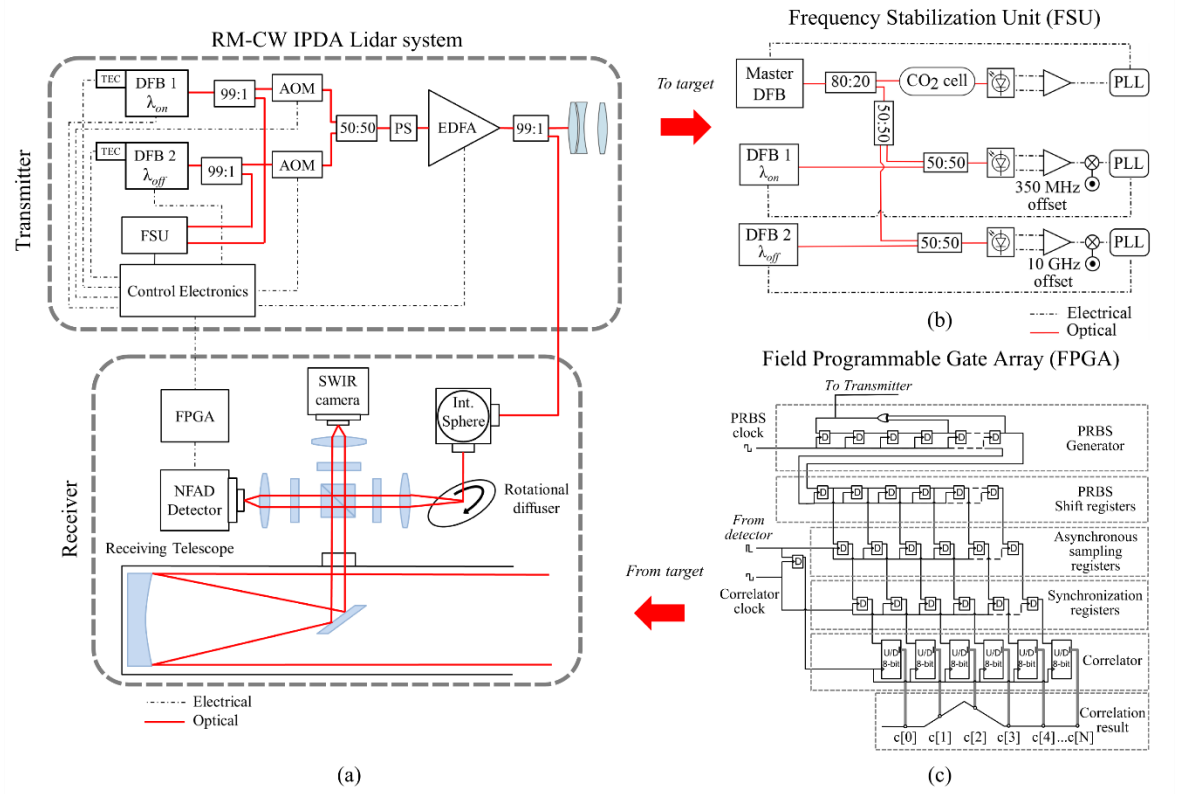

Fig. 2. (a) Schematics of the RM-CW IPDA lidar system composed by the transmitter (top) and the receiver (bottom). DFB: Distributed feedback laser. TEC: Thermo-electric cooler. AOM: Acousto-optic modulator. EDFA: Erbium doped fiber amplifier. FSU: Frequency stabilization unit. PS: Polarization scrambler. NFAD: Negative feedback avalanche diode. SWIR: Short-wave infrared. FPGA: Field programmable gate array. (b) Schematics of the FSU, based on three phase locking loops (PLLs). (c) FPGA asynchronous implementation of the PRBS generator and correlator, composed by D flip-flops and up/down (U/D) 8 bit counters.

B. Receiver

On the side of the receiver, the reflected light from the target is collected by a Newtonian telescope (diameter = 152.4 mm) with a field of view (FOV) of 200 µrad matching the laser beam divergence. Alignment issues are addressed by using a short-wave infrared (SWIR) camera. A very high sensitivity detector based on InGaAs negative feedback avalanche diode (NFAD) is used for SPC of the received signal. The NFAD is used in order to minimize the degradation of the SNR in comparison with pulsed systems due to the detector noise [16]. We have developed in-house our own single photon detector unit as commercial detectors do not satisfy our need of a high saturation count rate [17]. The detector achieves 5 Mcps with 100 kcps dark count with an efficiency of 10 %. It should be noticed, that the intrinsic NFAD non-linearity caused by detector dead-time can be completely canceled out, due to the fact that CO_2 concentration is calculated from the ratio between the on- and off-line received echoes [16]. The modulation sequence and the correlation process required by the RM-CW technique are implemented with a field programmable gate array (FPGA). Alternatively to other correlators, the FPGA implementation of the single photon correlator is based in an asynchronous design, see Fig. 2 (c). This presents modifications respect to the correlator presented in [18]. First of all the PRBS is generated by a first layer of linear feedback shift registers. A second layer of shift registers, acting as delay lines, records the PRBS signal. Once a photon is received, the rising edge of the photon trigger will latch the shift register contents into the flip-flop of the asynchronous sampling registers. Subsequent to this layer a synchronization registers layer is needed to deal with meta-stability. The last layer is the correlator elements that are just counters which increments with logic ‘1’ being seen at the second layer shift registers and decrement with ‘0’. The result of the correlation appears as a triangle where the addition of the two highest consecutive peaks (c[1] and c[2]) indicate the number of correlated photons.

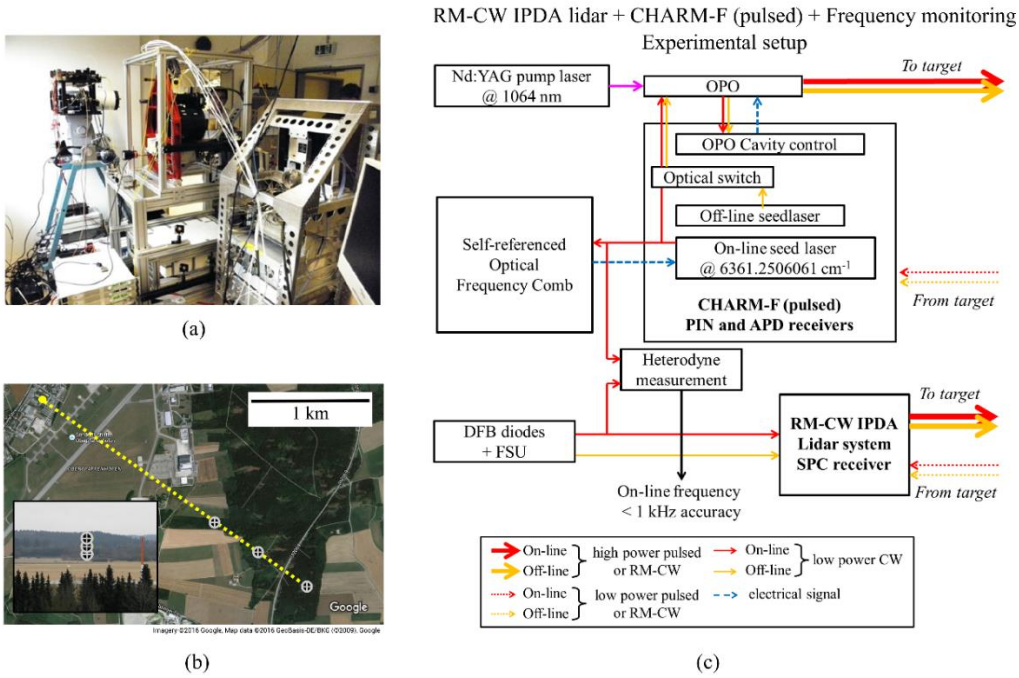

Fig. 3. (a) Photograph of the RM-CW IPDA lidar and CHARM-F instruments in the laboratory. (b) Map showing the trial path. The 2, 2.5 and 3 km path distances are indicated. Inset: view from the laboratory window. (c) Experimental setup consisting in both systems, the RM-CW IPDA and CHARM-F instruments, and the Optical Frequency Comb (OFC).

IV. EXPERIMENTAL SETUP

In order to test and demonstrate the validity of the RM-CW SPC IPDA lidar system for column-averaged CO_2 concentration measurement, a test campaign with co-located measurements with a pulsed system and an in-situ instrument was performed. The test campaign took place during February 2016 at the Institute of Atmospheric Physics, DLR Oberpfaffenhofen, Germany. The pulsed system, CHARM-F, is the result of a five-year in-house development [11], which aims to serve as a technology demonstrator for IPDA lidar measurements of the two main anthropogenic greenhouse gases, CO_2 and methane (CH_4). CHARM-F's laser sources (one for CO_2 and the other for CH_4) are based on injection-seeding of pulsed optical parametric oscillators (OPO) by a low-power, CW laser source, allowing to simultaneously achieve the very narrow bandwidths and high pulse energies required for the application. The OPOs are themselves pumped by Nd:YAG lasers producing double pulses at 1064 nm separated by only a few hundred ns at a rate of 50 Hz. A fast optical switch enables switching between the on-line and off-line seed laser in the short time between the two pulses. The spatial mismatch between on-line and off-line footprint on ground is thereby minimized, although not fully removed. In this aspect the RM-CW approach presents a clear advantage. Fig. 3 (a) shows both instruments in the laboratory, the RM-CW IPDA lidar and the CHARM-F system in its frame and the rack for the frequency reference and data acquisition subsystems. CHARM-F is equipped with two receivers per trace gas, one making use of a quadrant PIN photodiode and a reflective telescope with an aperture of 20 cm, the other making use of an avalanche photodiode (APD) at the focus of a refractive telescope of 6 cm aperture.

DLR's premises in Oberpfaffenhofen are placed in a rural setting, right next to an airfield, and thanks to a convenient position of the Institute with respect to the neighboring buildings, one window of the laboratories offers an obstacle-free view across the airfield to a forested area at a distance of around 2 km distance, as illustrated on Fig. 3 (b). Furthermore, the presence of a hill on the line of sight makes it possible to target trees at different ranges, from about 2 to 3 km. In addition to both IPDA lidar instruments, an in-situ instrument was also used. The in-situ instrument (LI-820 CO_2 gas analyzer) is based on a dual filter infrared detection system. By means of a long plastic pipe and existing feedthroughs between the laboratory and an astronomical cupola on the roof of the institute, the air was sampled directly above the lidar systems, providing a localized point measurement at the very beginning of the path.

The experimental setup is shown in Fig. 3 (c). It consists in both systems, the RM-CW IPDA and CHARM-F instruments, and a self-referenced optical frequency comb (OFC) (Menlo systems FC1500 Optical Frequency Synthesizer) with absolute long-term optical frequency stability better than 1 kHz, used for frequency monitoring

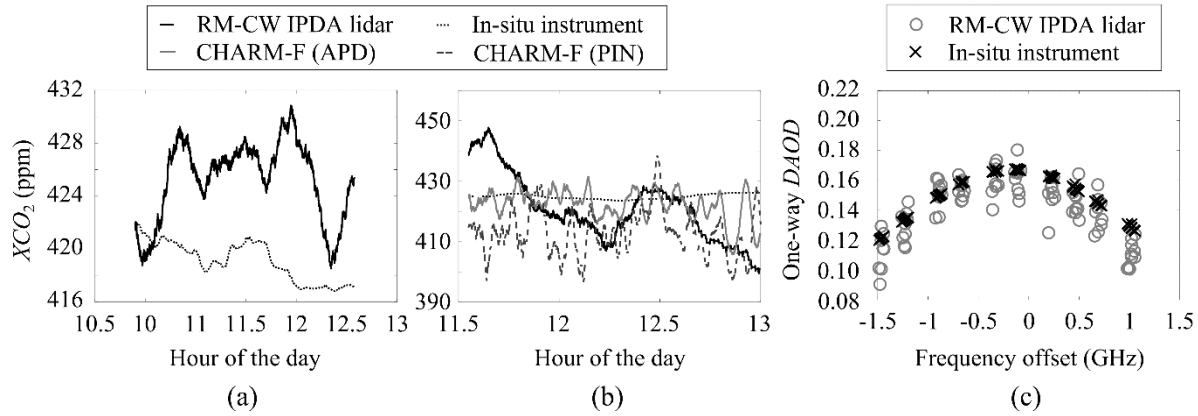

Fig. 4. Experimental results. CO_2 dry-air volume mixing ratio along the laser beam (XCO_2) measured with the different instruments: RM-CW IPDA lidar, in-situ instrument and CHARM-F. (a) 05/02/2016 and (b) 18/02/2016. (c) One-way differential absorption optical depth (*DAOD*) versus frequency offset with respect to the CO_2 line center in vacuum, measured with the RM-CW IPDA lidar and the expected values derived from the in-situ instrument. 17/02/2016.

and locking. As shown previously, the tests were performed in a horizontal path. In this case, (9) is greatly simplified compared to a down-looking IPDA measurement through many heterogeneous layers of the atmosphere. It can indeed be safely assumed that the pressure and temperature along the horizontal path are uniform, so (9) simplifies as

$$XCO_2 = \frac{DAOD}{Z\left[\sigma_{on}(p,T) - \sigma_{off}(p,T)\right] n_{air}(p,T)}, \tag{14}$$

being the *DAOD* calculated according to (1), the absorption cross-sections were computed using a Voigt profile and the latest line-by-line spectroscopic parameters from the HITRAN database [14]. Pressure and temperature were measured by an autonomous weather station permanently installed on the building's roof.

V. EXPERIMENTAL RESULTS

Fig. 4 (a) compares the measured XCO_2 with the RM-CW IPDA system and the in-situ instrument during the first phase of the test campaign at the beginning of February. The on-line laser of the RM-CW IPDA system was locked using the FSU. This experiment achieved the best match between the RM-CW IPDA system and the in-situ measurements, with a maximum discrepancy of 10 ppm over two hours. Other experiments performed in mid-February, Fig. 4 (b), show some strong time-varying offsets of the RM-CW IPDA system results in comparison with both the in-situ instrument and the CHARM-F data. Overall, time-varying offsets of up to ±10 % were observed on the RM-CW IPDA system results with respect to the in-situ data. Offsets were also present in the data of the pulsed system; however, both receivers of the CHARM-F had a small and roughly constant offset relative to each other of about 10 ppm and a constant offset of -20 ppm with respect to the in-situ instrument data, while the RM-CW IPDA system had a different offset (with a different sign). The constant offset can be satisfyingly explained by the uncertainty of ±10 ppm on the concentration of CO_2 in the reference mixture that was used to calibrate the in-situ instrument, on the one hand, and by the uncertainties in the HITRAN line parameters that were used to convert between XCO_2 and *DAOD* values through (14), on the other hand. As far as the remaining variations are concerned, some evidence points to speckle effects combined with the heterogeneous reflectivity of the target. First, the CHARM-F data exhibits larger instability when the local wind was weaker than on the previous days (not shown), producing less "blurring" of the speckle patterns through the movement of the trees. And second, the generally larger amplitude of the variations on the RM-CW system are consistent with a smaller number of speckles in the field of view, due to the system's smaller divergence.

Another type of experiment was also performed. In this case steps were applied to the temperature regulation of the free-running RM-CW IPDA on-line DFB laser, so as to measure the differential optical depth at different positions around the center of the absorption line. The results are presented on Fig. 4 (c). The correct overall shape and position was obtained, with a shift of the absorption line at ground pressure of about 200 MHz towards lower optical frequencies with respect to the line center in vacuum, as expected. However, the same variability of about ± 10 % in the absolute values of the measured *DAOD* was observed when comparing measurements at the same frequency position within the same scan experiment (as seen from the spread of the measurements within a column).

VI. CONCLUSIONS

An IPDA lidar system for atmospheric CO_2 measurement based on a hybrid MOPA and SPC receiving techniques has been proposed and demonstrated. Experiments in a horizontal path have been carried out and compared with a pulsed system and with an in-situ instrument. It has been found that a relative accuracy of the order of about ± 10 %, or ± 40 ppm CO_2 concentration in absolute terms, was achieved with the proposed RM-CW IPDA lidar system. These numbers are more than one order of magnitude away from the threshold requirement for a space-borne IPDA lidar mission for CO_2, however they should be put in perspective with the consideration that due to speckle effects, a horizontal measurement on a fixed target is a worst-case scenario compared to an air-borne or space-borne measurement with a continuously changing target. The measurements nevertheless qualitatively demonstrate the feasibility of CO_2 IPDA measurements with a RM-CW system. These systems can be implemented with recently demonstrated monolithically integrated MOPAs [6] together with SPC at the receiver for future space-borne lidar instruments.

ACKNOWLEDGMENT

This work was supported by the European Commission through the project FP7-SPACE BRITESPACE under grant agreement no. 313200. A. Pérez-Serrano and I. Esquivias also acknowledge support from the Ministerio de Economía y Competitividad of Spain under projects RANGER (TEC2012-38864-C03-02) and COMBINA (TEC2015-65212-C3-2-P); and the Comunidad de Madrid under program SINFOTON-CM (S2013/MIT-2790). A. Pérez-Serrano acknowledges support from Ayudas a la Formación Posdoctoral 2013 program (FPDI-2013-15740). P. Adamiec acknowledges support from the Torres Quevedo 2013 program (PTQ-13-06438).

REFERENCES

[1] G. Ehret, C. Kiemle, M. Wirth, A. Amediek, A. Fix, and S. Houweling, "Space-borne remote sensing of CO_2, CH_4, and N_2O by integrated path differential absorption lidar: A sensitivity analysis," *Appl. Phys. B*, vol. 90, pp. 593-608, 2008.
[2] P. Ingmann, P. Bensi, Y. Duran, A. Griva and P. Clissold, "A-SCOPE - Advanced space carbon and climate observation of planet Earth," ESA Report for assessment, SP-1313/1, 2008.
[3] J.B. Abshire, *et al*., "Pulsed airborne lidar measurements of atmospheric CO_2 column absorption," *Tellus Ser. B*, vol. 62, pp. 770-783, 2010.
[4] G.J. Koch, et al., "Coherent differential absorption lidar measurements of CO_2," *Appl. Opt*., vol. 43, pp. 5092-5099, 2004.
[5] M. Faugeron, *et al*., "High power three-section integrated master oscillator power amplifier at 1.5 µm," *IEEE Photon. Technol. Lett*., vol. 27, pp. 1449-1452, 2015.
[6] M.-C. Amann, T. Bosch, M. Lescure, R. Myllyla, and M. Rioux, "Laser ranging: A critical review of usual techniques for distance measurement," *Opt. Eng*., vol. 40, pp. 10-19, 2001.
[7] N. Takeuchi, N. Sugimoto, H. Baba, and K. Sakurai, "Random modulation cw lidar," *Appl. Opt*., vol. 22, pp. 1382-1386, 1983.
[8] P. Kapusta, M. Wahl, and R. Erdmann, *Advanced Photon Counting: Applications, Methods, Instrumentation*, Springer, 2015.
[9] J. Beck, T. Welch, P. Mitra, K. Reiff, X. Sun, and J. Abshire, "A highly sensitive multi-element HgCdTe e-APD detector for IPDA lidar applications," *J. Electron. Mater.*, vol. 43, pp. 2970-2977, 2014.
[10] www.britespace.eu
[11] A. Amediek, A. Fix, M. Wirth, and G. Ehret, "Development of an OPO system at 1.57 µm for integrated path dial measurement of atmospheric carbon dioxide," *Appl. Phys. B*, vol. 92, pp. 295-302, 2008.
[12] J.F. Campbell, N.S. Prasad, and M.A. Flood, "Pseudorandom noise code-based technique for thin-cloud discrimination with CO_2 and O_2 absorption measurements," *Opt. Eng*., vol. 50, pp. 126002-126002-8, 2011.
[13] J. Caron and Y. Durand, "Operating wavelengths optimization for a spaceborne lidar measuring atmospheric CO_2," *Appl. Opt*., vol. 48, pp. 5413-5422, 2009.
[14] L. Rothman, *et al.*, "The HITRAN2012 molecular spectroscopic database," *J. Quant. Spectrosc. Radiat. Transfer*, vol. 130, pp. 4 -- 50, 2013.
[15] X. Ai, *et al.*, "Analysis of a random modulation single photon counting differential absorption lidar system for space-borne atmospheric CO_2 sensing," *Opt. Express*, vol. 24, no. 18, pp. 21119-21133, 2016.
[16] X. Ai, *et al.*, "Pseudo-random single photon counting for space-borne atmospheric sensing applications," in *2014 IEEE Aerospace Conference*, March 2014.
[17] J.G. Rarity, *et al.*, "Single-photon counting for the 1300-1600-nm range by use of peltier-cooled and passively quenched InGaAs avalanche photodiodes," *Appl. Opt.*, vol. 39, pp. 6746-6753, 2000.
[18] X. Ai, R. Nock, J.G. Rarity, and N. Dahnoun, "High-resolution random-modulation cw lidar," *Appl. Opt.*, vol. 50, pp. 4478-4488, 2011.
[19] M. Quatrevalet, *et al.*, "Atmospheric CO_2 Sensing with a Random Modulation Continuous Wave Integrated Path Differential Absorption Lidar", submitted.